# A Relationship between Heme Binding and Protein Stability in Cytochrome $b_5$[†]

Kunal Mukhopadhyay and Juliette T. J. Lecomte*

*Department of Chemistry, The Pennsylvania State University, University Park, Pennsylvania 16802*

*Received May 29, 2004; Revised Manuscript Received July 10, 2004*

ABSTRACT: Conformational changes and long-range effects are often observed in proteins when they associate with their ligands. In many cases, these structural perturbations are essential to function, and they are the result of complex networks of interactions. Here we used cytochrome $b_5$, a protein that undergoes extensive structural rearrangement upon heme binding, to seek a relationship between affinity for the cofactor and extent of refolding induced by its binding. Three variants of the water-soluble domain of the rat microsomal protein were chosen to affect the stability of the apoprotein or the holoprotein. Sequence alterations were introduced in the heme binding loop (type I mutations, D60R and $^{55}$TENFED → $^{55}$TEPFEED, or PE), which is largely unstructured in the apoprotein state, and in the folded core of the apoprotein (type II mutation, P81A). Thermal and chemical denaturation experiments and heme transfer experiments were performed on these proteins. Type I mutations left the thermodynamic stability of the apoprotein unchanged. The first mutation (D60R) stabilized the holoprotein in a probable manifestation of enhanced helical propensity or improved electrostatic interactions. The second mutation (PE) decreased heme affinity and holoprotein stability in concert. For this protein, heme transfer experiments could be used to estimate the rate constant of heme loss from each of the heme orientational isomers. In contrast, the type II mutation resulted in a marked destabilization of the apoprotein but an intermediate effect on the holoprotein stability and heme affinity. These data supported that heme affinity could be modulated by the apoprotein stability and by specific residues remote from the heme binding site.

The ability of proteins to alter their conformational and dynamic properties as a result of association with substrates, cofactors, allosteric effectors, and other small molecules is often essential for their correct function. Although the importance of this modulation mechanism has been recognized for a long time, it remains a challenge to describe the ways in which binding at a specific site is controlled, how it is sensed throughout a structure, and how various parts of a protein communicate with one another in response to the association reaction (*1*−*4*). The thermodynamic contribution of conformational changes caused by binding can be accounted for in a simple Gibbs energy diagram. Figure 1A illustrates a lock-and-key model by which a fictitious apoprotein ($a'$) is fully folded into one cooperative unit and poised to establish the favorable interactions that the cofactor ($h$) will develop in the holoprotein ($H$) state. In Figure 1B, the apoprotein ($a$) is not properly conformed; compared to this state, the $a'$ state lies energetically uphill and is not necessarily populated under the same solution conditions. Interactions with the cofactor are fully developed from the $a'$ state, resulting in a net affinity for the cofactor lower in case B than in case A. Although of no mechanistic value (i.e., state $a'$ need not be on pathway in the association reaction (*3*, *5*)), this description of binding serves as a useful reference framework and suggests that induced refolding can provide a means of tuning cofactor affinity. Thus, by altering state $a$ so that structurally it resembles more closely the fictitious $a'$ state, a gain in net binding energy may be achieved.

Many heme-binding proteins undergo a conformational change upon associating with the heme as a cofactor (*6*−*8*) or a substrate (*9*). This perturbation, which is generally manifested in the refolding of secondary structural elements, in the repacking of side chains, and in distributed adjustments of internal motions, varies depending on the protein. For example, in sperm whale myoglobin, most of the structural changes are localized in the proximal region, in particular in and near the F helix (*10*), whereas in the cyanobacterial hemoglobin from *Synechocystis*, the apoprotein has molten globular properties under native conditions (*11*). At the other extreme of behavior, the hemophore HasA shows little conformational rearrangement upon binding its heme cargo (*12*). To understand better the determinants of structure in apo *b* hemoproteins and the range of behavior they display, it is necessary to explore the relationship among binding site preorganization, protein stability, and heme affinity.

Several factors contribute to the binding energy of the heme group (*13*). It is hydrophobic and partitions into a nonpolar protein interior in preference to aqueous solvent, but in the majority of *b* hemoproteins, the heme also establishes multiple specific interactions. These are coordination bond(s) to the iron ion, van der Waals contacts between the planar porphyrin ring and protein side chains, and electrostatic interactions involving the heme propionate substituents and positively charged protein residues. These interactions, which result in the preferential binding of heme and heme-like molecules, require a precise arrangement of protein backbone and side chains.

In the present work, we investigate aspects of stability and cofactor affinity with cytochrome $b_5$, a protein that exhibits

[†] Supported by National Institutes of Health Grant GM-54217.

* To whom correspondence should be addressed. Phone: (814) 863-1153. Fax: (814) 863-8403. E-mail: jtl1@psu.edu.

10.1021/bi0488956 CCC: $27.50 
Published on Web 08/28/2004

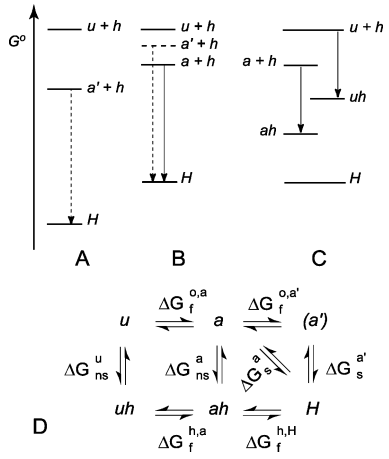


FIGURE 1: Free energy diagrams representing the different states of a hemoprotein. *H* is the holoprotein; *a′* is a fictitious apoprotein that is folded in a conformation requiring no rearrangement upon heme binding; *a* is the actual, partially folded apoprotein; *u* is the unfolded state; *ah* is a folded "apoprotein" state with heme nonspecifically bound; *uh* is an unfolded state with heme nonspecifically bound; *h* represents free heme. Native conditions, room temperature, and standard conditions of pressure and concentrations are assumed; the diagrams are not drawn to scale. In panel A ("lock-and-key"), the dashed arrow represents the affinity for the heme group. In panel B ("induced fit" or "conformational capture" scheme), the same energy is represented with a dashed arrow connecting the fictitious fully folded apoprotein state to the holoprotein state. The net affinity for the heme (solid arrow) is the difference between this maximum affinity and the $a \rightarrow a'$ refolding energy. In panel C, two additional states are included to allow for nonspecific association of the heme with folded (*ah*) and unfolded (*uh*) peptide. The down arrows indicate this nonspecific binding. In panel D, the various equilibria are represented with their Gibbs free energy differences. In each case, the final state lies on the right (horizontal steps) or at the bottom (vertical steps); the top row gives quantities in the absence of heme (superscript "o"); the bottom row gives quantities with an equimolar amount of heme (superscript "h"); vertical and diagonal processes refer to nonspecific (subscript "ns") or specific (subscript "s") heme binding energies. The hypothetical state *a′* is included for parallel with the scheme in panel B.

a striking apo to holo transition. The rat liver microsomal variant of interest contains a 98-residue water-soluble domain, which binds one molecule of iron−protoporphyrin IX with two axial ligands, His39 and His63. The holoprotein has an $\alpha\beta$ fold of complicated topology depicted in Figure 2 (*14*, *15*). The heme group is normally seated in an imperfect four-α-helical bundle, and this region of the structure requires the cofactor for maintenance of the fold. Specifically, the holoprotein secondary structure is described by elements $\beta$1-α1-$\beta$3-$\beta$4-α2-α3-$\beta$5-α4-α5-$\beta$2-α6 but is reduced in the apoprotein to $\beta$1-α1-$\beta$3-$\beta$4-α2-(α5)-$\beta$2-(α6), where parentheses indicate incomplete formation (*16*).

The holoprotein architecture contains two hydrophobic cores (*14*), core 1 comprising several residues of the heme binding pocket and core 2 consisting of residues remote from the heme site. The latter core is folded in the apoprotein (*7*) and forms a structural scaffold. This description is complemented by the analysis of backbone dynamics by NMR methods, which demonstrate a wide range of motional time scales in the disordered heme-binding site (*17*). Interestingly, one of the axial heme ligands to be, His39, appears confined to a small portion of the conformational space in the apoprotein, whereas the other, His63, samples a larger volume (*18*). The two residues have different p$K_a$'s (*19*) arising from

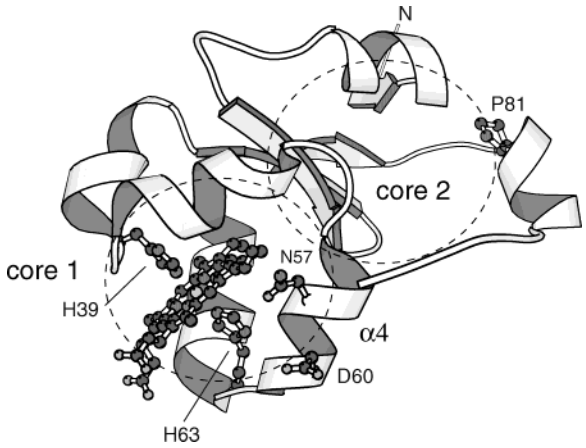


FIGURE 2: Minimized average NMR structure of the water-soluble domain of oxidized rat microsomal cytochrome $b_5$ (1aw3; *15*). Hydrophobic cores 1 and 2 (*14*) are indicated by circles. The residues of interest to this study are shown.

primary and higher-order structural differences and are thought to play distinct roles in the mechanism of heme binding (*20*).

Cytochrome $b_5$ denaturation is a cooperative process that is generally modeled by considering only two states. The cooperative unit encompasses the whole protein when the heme is present and only the scaffold of core 2 in its absence. With these two-state analyses, the apoprotein thermodynamic stability is several kilojoules lower than that of the holoprotein (*21*). Mutations in the scaffold can lower the midpoint of the apoprotein thermal denaturation transition (*22*). Not surprisingly, certain mutations in the heme-binding site can affect the affinity for the heme and destabilize the holoprotein (*23*). This is particularly obvious if a heme axial ligand is replaced (*16*, *20*, *24*). Here, we pursue amino acid replacements in the folded and unfolded regions of apocytochrome $b_5$. We chose two secondary structural elements for our analysis: α6, which in the wild-type holoprotein makes no contact with the heme group and is stabilized by an N-capping interaction compromised in the apoprotein (*25*), and α4, which ends with axial residue His63 and is largely unfolded in the apoprotein (*16*). Although the interpretation of *b* hemoprotein denaturation data requires departure from a simple two-state framework, our evaluation suggested a possible connection among the stabilities of the holoprotein and apoprotein and heme affinity and detected subtle long-range effects through the protein.

## MATERIALS AND METHODS

*Protein Expression and Purification.* The genes for D60R, P81A, and $^{55}$TENFED → $^{55}$TEPFEED (henceforth PE for short)[1] of rat microsomal cytochrome $b_5$ were obtained from the wild-type gene (*18*) using a PCR mutagenesis protocol

[1] Abbreviations: 2QF-COSY, double-quantum-filtered correlated spectroscopy; CD, circular dichroism; DEAE, diethylaminoethane; EDTA, ethylenediaminetetraacetic acid; ESI, electrospray ionization; IPTG, isopropyl $\beta$-thiogalactoside; MRE, molar residual ellipticity; NOESY, nuclear Overhauser effect spectroscopy; PCR, polymerase chain reaction; PE, replacement and insertion $^{55}$TENFED → $^{55}$TEPFEED; SDS−PAGE, sodium dodecyl sulfate polyacrylamide gel electrophoresis; TOCSY, totally correlated spectroscopy; Tris, tris(hydroxymethyl)aminomethane; WATERGATE, water suppression by gradient-tailored excitation.

based on the QuickChange method (Stratagene, La Jolla, CA). Oligonucleotides were purchased from Integrated DNA Technologies Inc. (Coralville, IA). Plasmids were introduced into competent DH5α *Escherichia coli* cells; after replication and purification (Qiagen Plasmid Miniprep Kit, Qiagen, Valencia, CA), the DNA sequences were confirmed at the Penn State Nucleic Acid Facility (University Park, PA). Further steps were essentially as described elsewhere (*16*, *18*). Plasmid DNA was introduced into BL21 DE3 *E. coli* cells (Novagen, Madison, WI), which were grown in M9 minimal medium in the presence of ampicillin (0.05 mg/mL). Protein expression was induced using IPTG (final concentration of 0.5 mM) when the optical density of the cell culture was approximately 0.8 at 600 nm. Cells were allowed to grow for an additional 5−6 h postinduction. The cell pellets obtained by centrifugation were resuspended in buffer (50 mM Tris, 1 mM EDTA, pH 7.5) and subsequently lysed by ultrasonication (Fisher Scientific, Pittsburgh, PA; model 60 sonic dismembrator). The cell-free extract was centrifuged, and the supernatant was titrated with a concentrated (50 mg/mL in 0.1 M NaOH) bovine hemin (Sigma-Aldrich Chemicals, St. Louis, MO) solution. Excess heme was removed by centrifugation after lowering the pH to 6. The supernatant was filtered through a 0.45 $\mu$m Tuffryn membrane filter (Pall Corp., Ann Arbor, MI) and further purified on a DEAE Sephacel anion-exchange chromatography column (Amersham Biosciences, Piscataway, NJ) using a NaCl gradient (0−0.4 M NaCl in buffer for elution. Additional purification was performed using a G-50 fine resin size-exclusion chromatography column (Amersham Biosciences) and was verified by SDS−PAGE (>95% pure). UV−vis spectrophotometry returned $A_{414}/A_{280}$ ratios higher than 6. Typical yields were about 50 mg of pure holoprotein per liter of growth medium. The purity and identity of each protein were confirmed by ESI mass spectrometry analysis.

Ferric holoprotein concentrations were estimated using an extinction coefficient ($\epsilon$) of 130 $mM^{-1}\,cm^{-1}$ at the Soret maximum (*26*). Because heme binding appeared abnormal in the PE variant, its $\epsilon$ value was confirmed with the hemochromogen assay (*27*, *28*). The result was 131 ± 3 $mM^{-1}\,cm^{-1}$ at 413 nm, within error of the wild-type protein.

Apoproteins were prepared from their respective holoproteins by repeated extraction of heme with butanone under acidic (pH 2.5) conditions (*29*). After extensive dialysis against water, the apoprotein solutions were either lyophilized or exchanged in buffer for immediate use. Apoprotein concentrations were calculated with $\epsilon = 10.6\ mM^{-1}\,cm^{-1}$ at 280 nm (*30*).

*Thermal Denaturation.* Apoprotein samples (≤100 $\mu$M) and holoprotein samples (≤10 $\mu$M) were prepared in 20 mM phosphate buffer, pH 7.2. UV−visible data were collected on an AVIV (Lakewood, NJ) model 14 DS spectrophotometer equipped with a Pelletier thermoelectric device for temperature control. Spectra (440−260 nm) were obtained every 2 °C starting at 10 °C up to 90 °C with an equilibration period of 3 min, which was verified to be sufficient. The reversibility of the unfolding reaction was tested by returning to the starting temperature while collecting spectra every 2 °C. Reversibility was 95−100% for all apoproteins and 70% and below for the holoproteins. For the apoproteins, the maximum difference in absorbance upon unfolding occurred at wavelengths between 283 and 287 nm. For the holoproteins, the Soret maximum (413 nm) was used. Data were analyzed by fitting to a modified Gibbs−Helmholtz equation as described elsewhere (*31*−*33*) using NFIT (University of Texas, Galveston, TX). In the fitting, $\Delta C_p$ was held constant at 6.2 (holoproteins) and 4.2 kJ $mol^{-1}\ K^{-1}$ (apoproteins). These values (*21*) were expected to be close to the actual value and when changed within reason did not influence the results significantly.

*Urea Denaturation.* Stock solutions of high concentration (∼10 M) urea (Ultrapure Urea, ICN Biochemicals Inc., Aurora, OH) were prepared and purified on a mixed bed resin column (Bio-Rad Laboratories Inc., Hercules, CA). Aliquots were either used immediately or frozen at −20 °C for later experiments. Titrations were performed with a computer-controlled Hamilton Microlab titrator. The protein concentration was 10−25 $\mu$M in 20 mM phosphate buffer (pH ≈ 7.4), and the samples were maintained at 25 °C. The urea concentration in the denatured protein solution (∼9.5 M) and in the protein solution at the end of the titration was determined by measuring the refractive indices of the solution with a Leica (Bannockburn, IL) Abbe Mark II Plus refractometer (*33*, *34*). In all titrations, two protein solutions of the same concentration were used, one with denaturant and one without. The titration started with the denaturant-free protein solution in the cuvette placed in the spectropolarimeter. After data were collected, a predetermined volume of solution was removed from the cuvette and replaced with an equal volume of denatured protein solution. The mixture was left to equilibrate for 5 min with stirring, data were collected, and the procedure was repeated. This titration protocol was found to be satisfactory when compared to manual titrations performed with an equilibration time of 20 h as reported by others (*35*). Far-UV circular dichroism spectra were collected from 210 to 250 nm on an AVIV model 62 DS circular dichroism spectropolarimeter. Raw data were corrected by subtracting values collected for buffer over the same wavelength interval and converted into molar residual ellipticity (MRE). Data analysis was performed using MRE values at 222 or 223 nm and the program SAVUKA (*36*). A linear free energy relation and a two-state equation (*33*) were used to fit the MRE data.

*Thermodynamic Analysis of Denaturation.* The two-state analyses imposed on the data yield an apparent fraction $F$ of folded protein given by

$$F = \frac{1}{1 + K_U} \tag{1}$$

In the case of the apoprotein, the denaturation process is represented by $a \leftrightarrows u$, $K_U$ is equal to $1/K_f^{o,a}$, and the standard Gibbs free energy associated with $K_U$ is $-\Delta G_f^{o,a}$ in Figure 1D. In the case of the holoprotein monitored in the Soret band, $K_U$ is a complex ad hoc parameter because the process involves more than two states (Figure 1C,D). In terms of species concentrations, the apparent fraction of folded holoprotein is, at the simplest,

$$F_H = \frac{[H]}{[H] + [a] + [ah] + [u] + [uh]} \tag{2}$$

where [H] stands for holoprotein concentration, regardless of heme orientation (see below). Equation 2 assumes that

(i) there are no folding intermediates and that (ii) because the solutions are dilute and the protein/heme ratio is equal to 1, there are no additional equilibria involving the heme group. At this stage, further assumptions are made: (iii) [a] $\ll$ [ah] and [u] $\ll$ [uh] owing to the low solubility of heme in aqueous solutions and its high nonspecific affinity for proteins and (iv) species *ah* and *uh* have identical heme optical properties. Equation 2 can be recast in a partition function ($Q$) format using [H] as the reference concentration and simplified to

$$F_H = \frac{1}{Q} = \frac{1}{1 + \frac{K_{ns}^a}{K_s^a} + \frac{K_{ns}^u}{K_s^a K_f^{o,a}}} \quad (3)$$

where the equilibrium constants refer to the nonspecific association of heme with folded apoprotein ($K_{ns}^a$) or unfolded protein ($K_{ns}^u$), the specific binding of heme to folded apoprotein ($K_s^a$), and the folding of the apoprotein ($K_f^{o,a}$). Equation 3 captures the observation that no protein concentration dependence is observed in the denaturation experiments. The constants in $Q$ are functions of temperature and denaturant concentration; as the conditions change, the weight of the two terms in which they participate varies. For holoproteins with a thermally stable apoprotein, $K_f^{o,a}$ is large under native conditions and $K_U$(25 °C) is close to the ratio of nonspecific to specific binding constants of heme to folded apoprotein (*37*). For variants with unstable apoprotein, $K_f^{o,a}$ is small, and the third term in $Q$ is not negligible. For example, if $K_f^{o,a}$(25 °C) = 1 and a single nonspecific association constant applies ($K_{ns}^a = K_{ns}^u = K_{ns}$), $K_U = 2K_{ns}/K_s^a$ and $\Delta G_U$ underestimates $\Delta G_{ns} - \Delta G_s^a$ by 1.7 kJ mol$^{-1}$. The interpretation of $T_m$ and $\Delta G_U$ is therefore not straightforward.

In the case of the holoprotein monitored for the presence of secondary structure, the observed signal is contributed by *H*, *ah*, and *uh*. Two-state behavior is expected if the stabilities are such that when the heme dissociates the apoprotein finds itself under strongly denaturing conditions. If the apoprotein and holoprotein thermal denaturation curves overlap, *ah* may be populated through the transition. Intermediates with specifically bound heme but partially folded protein (*iH* species) could also be present and affect the curves.

*NMR Spectroscopy.* All NMR data were collected on a Bruker DRX-600 spectrometer (14.1 T, operating at a $^1$H frequency of 600.05 MHz). For assignment purposes, sample concentrations were between 1 and 2 mM (20 mM phosphate buffer, pH 7.2−7.5, 25 °C). Two-dimensional NMR experiments (2QF-COSY, relaxation compensated TOCSY, and NOESY) were performed as detailed in prior work (*17*) with adjustment for the field strength as necessary. Water suppression was achieved by presaturation or with a WATERGATE sequence (*38*, *39*). Data were analyzed using XWIN-NMR (Bruker BioSpin, Rheinstetten, Germany).

*Heme Transfer Experiments.* These experiments were used to rank the variants according to their heme affinity at 25 °C. Pairs of heme donor and acceptor proteins were selected that have distinct hyperfine holoprotein $^1$H NMR spectra. Separate solutions of acceptor and donor proteins were prepared with concentrations ranging between 0.5 and 1.7 mM (20 mM phosphate buffer, $^1H_2O$ 90%/$^2H_2O$ 10%, pH 7.2−7.5). For example, in the holo PE/apo wild-type transfer experiments, four different sets of final concentration of proteins were studied, comprised of two sets of excess of holo PE (1.07 mM/0.91 mM and 0.65 mM/0.48 mM), an excess of the apo wild-type protein (0.71 mM/1.69 mM), and near-equivalent concentrations of both proteins (0.47 mM/0.52 mM).

Typically, a known volume of one of the two solutions was delivered to an NMR tube. The partner protein was then added in appropriate volume to obtain the desired final concentrations of the two proteins; the resulting solution was mixed, and NMR data collection was initiated as rapidly as possible. Successive one-dimensional spectra were recorded over a period of 24−48 h. At first, data were accumulated over consecutive 3-min periods with a recycling time ensuring the correct integration of the heme signals. At later times, the number of transients was doubled to improve the signal-to-noise ratio, and the spectra were separated by longer delays.

UV−vis absorption spectra of the stock solution of the donor protein, stock solution of the acceptor protein, and NMR sample after the transfer period were recorded. Because the apo and holoprotein optical spectra were not affected by the mutation and there was no free heme in solution either at the beginning or at the end of the experiment, the spectrum of the equilibrated mixture could, as a control, be deconvoluted into a holoprotein component (measuring total heme and reflecting the initial concentration of the donor protein) and an apoprotein component (measuring the initial acceptor protein concentration).

NMR data were processed with 20-Hz line broadening. The signals of interest were simulated in each spectrum with a set of adjustable Lorentzian lines using the program DmFit (*40*). Peak areas were attributed a time value corresponding to the middle of the acquisition period for that spectrum on the observation that the heme transfer was slow enough to result in a linear dependence of the concentrations over that period.

Heme transfer is represented as holo-donor + apo-acceptor $\leftrightarrows$ apo-donor + holo-acceptor or

$$DH + A \leftrightarrows D + AH \quad (4)$$

The apparent equilibrium constant for heme dissociation from a donor holoprotein is given by

$$K_1 = \frac{[D][h]}{[DH]} \quad (5a)$$

where h represents the free heme group. Similarly, the apparent equilibrium constant for the dissociation of heme from the acceptor protein is

$$K_2 = \frac{[A][h]}{[AH]} \quad (5b)$$

In mixtures of donor and acceptor proteins, [h] is common to both equilibria, and hence the ratio of the two constants can be reduced to

$$\frac{K_1}{K_2} = \frac{[D][AH]}{[DH][A]} \quad (6)$$

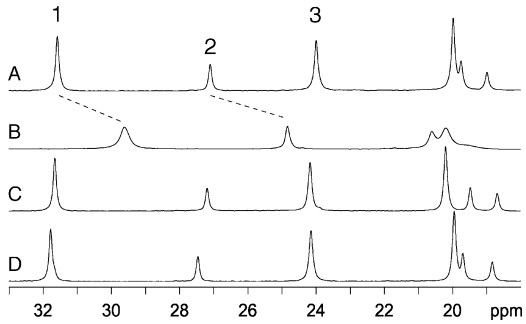


FIGURE 3: Downfield hyperfine-shifted region of the $^1$H NMR spectrum of (A) wild-type, (B) PE, (C) P81A, and (D) D60R holocytochrome $b_5$. Peaks labeled 1, 2, and 3 correspond to the heme 3-$CH_3$ of the minor (or B) isomer, the heme 2α-vinyl of the major (or A) isomer, and the heme 8-$CH_3$ of the minor isomer, respectively. PE holocytochrome $b_5$ exhibits broad and shifted lines compared to the other spectra. Dashed lines connect peaks with identical assignments in PE and the wild-type protein. Conditions were pH ≈ 7.2, 25 °C, 1.0−2.5 mM protein.

The $K_1$ and $K_2$ constants are apparent quantities in part because for each holoprotein there are two possible heme orientations within the binding site, yielding isomer A ($DH_A$ or $AH_A$) and isomer B ($DH_B$ or $AH_B$) having different heme affinities; the holoprotein concentrations are therefore [DH] = [$DH_A$] + [$DH_B$] and [AH] = [$AH_A$] + [$AH_B$]. In eqs 5a and 5b, no discrimination was made for the A and B isomers. Although eq 6 was applied to rank the variants, the ratio $K_1/K_2$ was not used quantitatively because of the large errors originating from concentration determinations.

The time course of the concentrations during heme transfer can be reproduced with four reversible heme loss steps, one for each of the possible holoproteins, for example,

$$DH_A \underset{k_{on,D_A}}{\overset{k_{off,D_A}}{\rightleftharpoons}} D + h \qquad (7a-d)$$

This set of phenomenological equations does not account for all states that may be transiently formed in solution. For example, heme reorientation is expected to involve species that do not release the heme completely in solution (similar to state *ah* mentioned above). In addition, direct interactions between donor and acceptor proteins are possible. Nevertheless, the simplified interpretation of the transfer reaction resulted in satisfactory fits and allowed for the determination of the rate of heme loss from PE cytochrome $b_5$. The evolution of the relative concentrations throughout the exchange process was simulated using the software KinTekSim (*41*, *42*).

## RESULTS AND DISCUSSION

*Wild-Type Cytochrome $b_5$.* Ferric holocytochrome $b_5$ gives high-quality NMR spectra that have been extensively analyzed by others (*43*, *44*). The downfield region containing hyperfine-shifted signals used in this work is shown in Figure 3. This figure also illustrates the presence of the heme orientational isomers commonly found in *b* hemoproteins. The two forms are related by a rotation of 180° around the α,γ-meso axis of the heme (*45*) as schematized in Figure 4. Spectral assignments are available for both isomers (*46*, *47*) and the A/B isomer ratio can be determined by comparing the integrated intensity of the 3-$CH_3$ B signal and the 2-α-vinyl A signal (Figure 3). In the equilibrated

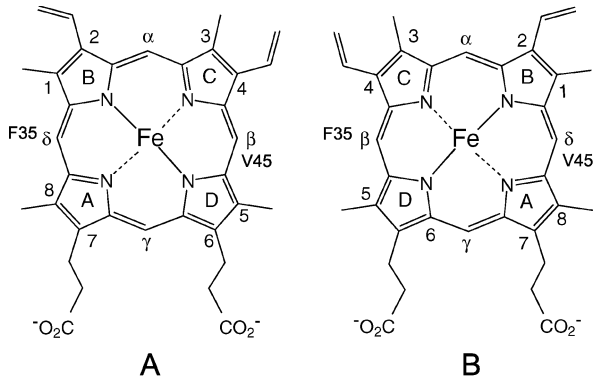


FIGURE 4: Structure of the heme group with the nomenclature used in this work. The major (A) and minor (B) heme orientational isomers are related by a 180° rotation about the α,γ-meso axis. They are defined with respect to position in the protein, with the A isomer having Phe35 on the δ meso side of the heme and Val45 on the β meso side. The B isomer has the interchanged heme/protein relationship.

samples considered here, the A/B ratio was ∼3:2 at neutral pH and 25 °C, as reported by others (*43*). Immediately after reconstitution of the apoprotein with heme, the ratio of heme isomers was nearly 1:1 (not shown). The reorientation process in the wild-type protein required days at neutral pH.

The thermal denaturation of apocytochrome $b_5$ is reversible, and reliable thermodynamic data based on a two-state analysis can be extracted from the curves (*16*, *21*−*23*). The experiment yields the standard Gibbs energy difference between *a* and *u* in Figure 1. The thermal unfolding of the wild-type holoprotein was monitored for comparison with other proteins studied in the present work. In the simplest model that couples binding with refolding, the denaturation process would yield the Gibbs energy difference between *H* and *u*+*h* in Figure 1B, and a dependence on concentration would be observed. However, this model is not appropriate because of the fate of the heme, which remains nonspecifically associated with the polypeptide under a wide range of conditions. Nonspecifically associated states have been considered in the unfolding of cytochrome $b_{562}$ (*48*), cytochrome $b_5$ (*23*) and myoglobin (*49*−*51*) and are included in Figure 1C,D as *uh* and *ah*. In effect, these states can decouple apoprotein and holoprotein stability (*37*). In addition to this complicating factor, other considerations apply: The holoprotein is a mixture of A and B isomers generally endowed with different heme affinity, and empirically, the thermal process is not completely reversible. Because of these peculiarities of *b* hemoproteins, estimated Gibbs free energy differences based on two-state analyses are often provided only as a means to compare curves collected under the same experimental protocol, a practice that will be followed here. Table 1 contains the relevant information.

*PE Cytochrome $b_5$.* For our purposes, the tested variants are classified into type I and type II depending on the proximity of the mutation to core 1 (almost completely unfolded in the apoprotein state) or core 2 (almost completely folded in the apoprotein state), respectively. Helix α4 ($^{55}$TENFED), which precedes one of the ligating histidine residues (H63), has a low propensity to form (*52*, *53*). We opted to reduce this propensity further by changing one residue (N57→P) and inserting another (E between E59 and D60) to obtain the sequence $^{55}$TEPFEED. This type I variant

Table 1: Denaturation Parameters for Cytochrome $b_5$ Variants

| | $T_m$ (°C)[a] | | $\Delta H°$ at $T_m$ | | $\Delta G°$[b] | | holo | |
|---|---|---|---|---|---|---|---|---|
| | holo | apo | holo[d] | apo | holo[d] | apo | $m$[c] | $\Delta G°$[b] |
| WT | 70.0 ± 0.1 | 46.1 ± 0.6 | 345 ± 10 | 142 ± 6 | 26.2 ± 1.4 | 6.4 ± 0.4 | 3.9 ± 0.1 | 27.5 ± 0.8 |
| PE | 58.0 ± 0.1 | 44.5 ± 0.3 | 299 ± 1 | 139 ± 6 | 19.3 ± 0.1 | 6.1 ± 0.5 | 4.4 ± 0.2 | 20.0 ± 0.8 |
| P81A | 63.3 ± 0.1 | 25.7 ± 0.7 | 329 ± 6 | 62 ± 10 | 23.5 ± 0.7 | 0.1 ± 0.1 | 4.4 ± 0.2 | 22.7 ± 0.8 |
| D60R | 76.0 ± 0.1 | 46.9 ± 0.8 | 354 ± 8 | 150 ± 6 | 27.6 ± 1.1 | 7.0 ± 0.6 | *e* | >27.5[e] |

[a] Midpoint of the thermal denaturation (20 mM phosphate, pH 7.2). Errors for $T_m$ and other quantities are from multiple runs. [b] In kJ mol$^{-1}$, at 25 °C, and in the absence of urea. [c] In kJ mol$^{-1}$ M$^{-1}$. [d] These values are provided only as a way to compare the curves (see Materials and Methods). [e] The data did not allow for an accurate determination of the unfolded baseline.

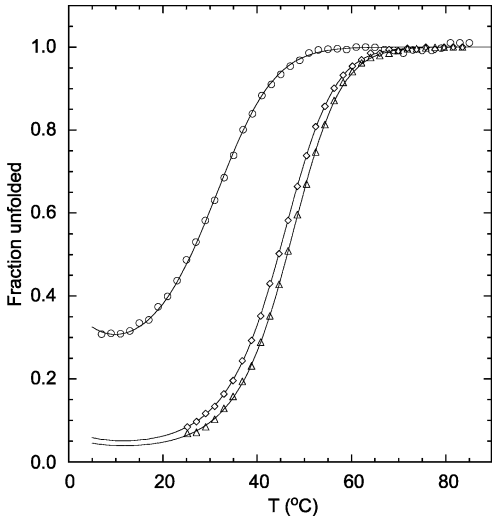


FIGURE 5: Thermal unfolding of D60R (△), PE (◇), and P81A (○) apocytochrome $b_5$ monitored by UV absorbance spectroscopy. The data were converted into a normalized plot using a two-state model. The solid lines represent the result of the fits (Table 1). The curve for the wild-type apoprotein falls between the PE and D60R curves and is omitted for clarity. Conditions were pH 7.2 in 20 mM phosphate buffer with protein concentrations ≤100 μM.

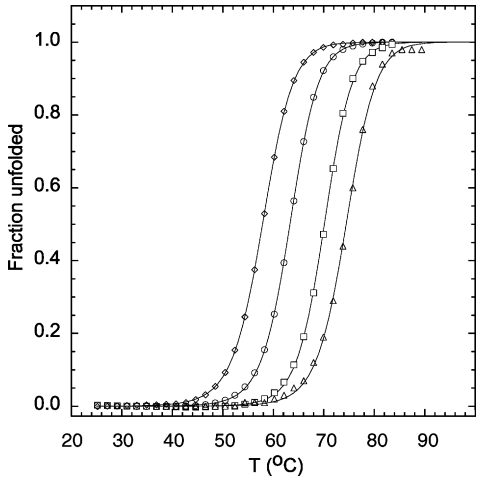


FIGURE 6: Thermal denaturation of wild-type (□), D60R (△), PE (◇), and P81A (○) holocytochrome $b_5$. The absorbance signal was monitored at 413 nm as a function of temperature. The change in the intensity of the Soret band illustrates the decoordination of His39 and His63 from the heme iron. The data were converted into a normalized plot using a two-state model. The solid lines represent the result of the fits (Table 1). Conditions were pH 7.2 in 20 mM phosphate with protein concentrations ~10 μM.

is referred to as PE cytochrome $b_5$. The proton NMR spectra of PE apocytochrome $b_5$ were practically indistinguishable from those of wild-type apocytochrome $b_5$ (not shown). Figure 5 illustrates the denaturation curve, which was within error of that from the wild-type protein (Table 1). These observations supported the view that an alteration of the sequence in the disordered region of the apoprotein had no consequence for the thermodynamic stability of the folded core, and it therefore argued for independence of the two protein regions.

Ferric PE holocytochrome $b_5$ showed an NMR spectrum that was significantly perturbed (Figure 3), a useful property in the heme transfer experiments described below. Differences were observed in hyperfine shifts and line widths, the latter feature suggesting changes in the dynamic properties of the protein. Two-dimensional NMR data were recorded to assign the heme signals in a procedure typically used for hemoglobins and cytochromes (*54*). It was determined that the two most shifted signals in Figure 3B corresponded to the 3-$CH_3$ in the B isomer and the 2-α-vinyl in the A isomer, as in the wild-type spectrum. Integration of these peaks returned an A/B value of 3:2, unchanged compared to the wild-type ratio. Remarkably, although helix α4 was likely disrupted and the register of one of the axial residues (His63) had changed, the heme was still bound in a low-spin ($S = {}^1/_2$) fashion, and cyanide ions, when used in large excess, did not displace His63 or His39.

Thermal and chemical (urea) denaturation experiments (Figures 6 and 7, Table 1) revealed the lower stability of PE holocytochrome $b_5$ compared to the wild-type protein ($\Delta T_m \approx -12$ °C and $\Delta C_m = -2.4$ M). In the thermal experiments, heme was lost from the mutant holoprotein under conditions that were not fully denaturing to the apoprotein (Figures 5 and 6). Data simulations were performed with the assumption that the *ah* ⇆ *uh* equilibrium shared the properties of the *a* ⇆ *u* equilibrium determined via apoprotein denaturation; they established that the presence of the ah species did not contribute significantly to the properties of the curve displayed in Figure 6. In addition, when the thermal denaturation was followed through changes in ellipticity at 220−224 nm (not shown), the onset of the transition occurred at lower temperatures than that observed with the Soret band, an indication that the secondary structure of the heme binding site may unravel readily in this variant. These aspects of the PE protein will be pursued elsewhere.

*D60R Cytochrome $b_5$.* A second type I variant (D60R) was designed to increase the helical propensity of α4. NMR data recorded on the corresponding apo- and holoprotein suggested no obvious structural differences compared to the wild-type forms. Denaturing profiles indicated that the apoprotein was as stable as the wild-type protein, as expected for a type I mutation. In contrast, the holoprotein had a $T_m$ elevated by 5 °C over the wild-type protein (Figure 6, Table 1). The chemical denaturation of the holoprotein monitored

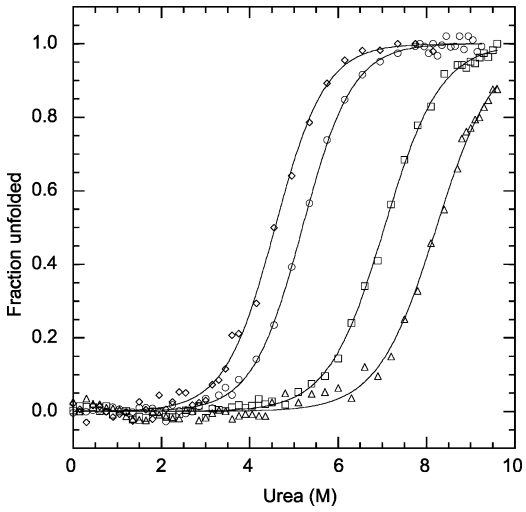


FIGURE 7: Urea denaturation of wild-type (□), D60R (△), PE (◇), and P81A (○) holocytochrome $b_5$. The ellipticity was monitored at 222 nm as a function of urea concentration. The data were converted into a normalized plot using a two-state model. The solid lines represent the result of the fits (Table 1). The line for the D60R protein was drawn with parameters $m = 3.7$ kJ mol$^{-1}$ M$^{-1}$ and $\Delta G° = 30.6$ kJ mol$^{-1}$ to aid the eye. One representative data set is shown per protein. Conditions were pH 7.2 in 20 mM phosphate with protein concentrations between 10 and 25 $\mu$M.

by CD suggested enhanced thermodynamic stability as well (Figure 7).

*P81A Cytochrome $b_5$*. The α6 helix of wild-type cytochrome $b_5$ starts with the sequence $^{80}$HPDD and features an N-capping H-bond between the ring of His80 (N$\delta$) and the backbone amide hydrogen of Asp82 in the holoprotein state. In the apoprotein, the N-capping interaction is kinetically labile, and α6 exhibits slow conformational exchange on the NMR chemical shift time scale (*25*). Because α6 is remote from the heme binding site (Figure 2), its behavior illustrates the long-range influence of heme binding. In prior work, it was found that the double replacement H80A/P81A resulted in a marked destabilization of the apoprotein despite the use of residues favoring helical formation (*22*). In light of these results, the type II P81A single mutant was chosen.

The thermal denaturation of the P81A apocytochrome $b_5$ is illustrated in Figure 5. As observed for the other variants, the transition was completely reversible; however, the P81A apoprotein had such a low stability that the unfolded state was significantly populated even at low temperature. The destabilization was confirmed by NMR analysis, which provided a spectrum typical of a mostly disordered protein at 25 °C. Ferric P81A holocytochrome $b_5$ had a wild-type-like $^1$H NMR spectrum (Figure 3). The similarity demonstrated negligible perturbation of the heme electronic structure and therefore the structure of the binding site. Assignments of the resolved signals were obtained by homonuclear methods and the ratio of isomers (A/B) at equilibrium was found to be unaltered. Compared to the wild-type holoprotein, P81A holocytochrome $b_5$ was moderately destabilized. The apo- and holoprotein denaturation transitions were well separated, but the marginal stability of the apoprotein implied that the holoprotein thermal denaturation curve was shifted to lower temperatures in part because of this property (see Materials and Methods).

Based on the $T_m$'s estimated from thermal denaturation experiments, the stabilities of holoproteins were in the order D60R > wild-type > P81A > PE; this order was also established with chemical denaturation. The apoprotein stabilities were in the order wild-type ≈ PE ≈ D60R > P81A.

*Heme Transfer Experiments*. The denaturation results confirmed that an amino acid replacement could have differential effects on the holo and apoprotein states. We considered next the consequences for heme affinity. Equation 3 and the ordering provided above suggested that heme affinity should vary in the order D60R > wild-type > P81A > PE, in concert with holoprotein stability. This expectation assumed that the properties of species *ah* were not significantly affected by the changes in sequences. To establish a relative scale of heme affinity, heme partitioning experiments were performed. A solution of heme-bound protein (holoprotein, donor, DH) and a solution of heme-free protein (apoprotein, acceptor, A) were mixed, and the heme transfer from the donor to the acceptor protein (eq 4) was monitored by NMR spectroscopy. In the majority of experiments, PE holocytochrome $b_5$ was chosen as the donor because of its anticipated low heme affinity and its distinctive heme signals (Figure 3).

The concentration of each heme-containing species (DH and AH, distributed in minor and major isomers) was obtained as a function of time by simulation of five heme resonances in the $^1$H spectrum (resolved in Figure 3; labeled 1, 2, and 3 in the wild-type spectrum, and 1 and 2 in the PE spectrum). The total heme concentration, represented by the appropriately weighted sum of these numbers, was constant over the course of the experiment (deviation smaller than 5%), which indicated the absence of free heme in the holoprotein preparations. After a period of time, the concentrations of the donor holoprotein (DH) and the acceptor holoprotein (AH) reached a steady state. At this point, the AH and DH concentrations reported on the relative heme affinity. The equilibration of A and B isomers within the acceptor protein required longer incubation times as will be seen below.

*PE Holocytochrome $b_5$ Plus Wild-Type Apocytochrome $b_5$*. When PE holocytochrome $b_5$ was mixed with the wild-type apoprotein, heme transfer was clearly demonstrated by losses in the intensity of peaks corresponding to the PE holocytochrome $b_5$ (curves x and y in Figure 8) and gains in the intensity of peaks corresponding to wild-type holocytochrome $b_5$ (curves p and q in Figure 8). The conditions for Figure 8A represented an excess of the donor over acceptor protein. Heme transfer was completed within 3 h at neutral pH. Beyond that time, curves p and q illustrated heme reorientation. In separate experiments, the concentrations of donor and acceptor proteins were varied (e.g., Figure 8B).

In all cases, the loss of heme from the donor protein occurred faster from the minor isomer (curve y) than the major isomer (curve x). With a simple mechanism of heme transfer (eqs 4 and 7a−d), a rate constant for heme loss ($k_{off}$) can be estimated for each of the A and B isomers. These values were ∼0.02 min$^{-1}$ and ∼0.03 min$^{-1}$, respectively. The ratio of these rate constants matched that of the initial isomer concentrations and indicated that the relative affinity for the heme group was controlled by $k_{off}$. It is interesting to note that isomer B of the acceptor protein appeared to be populated at a faster rate than isomer A. This initial incongruity in rates led to an excess of the B isomer, which was dissipated after a period of equilibration by conversion

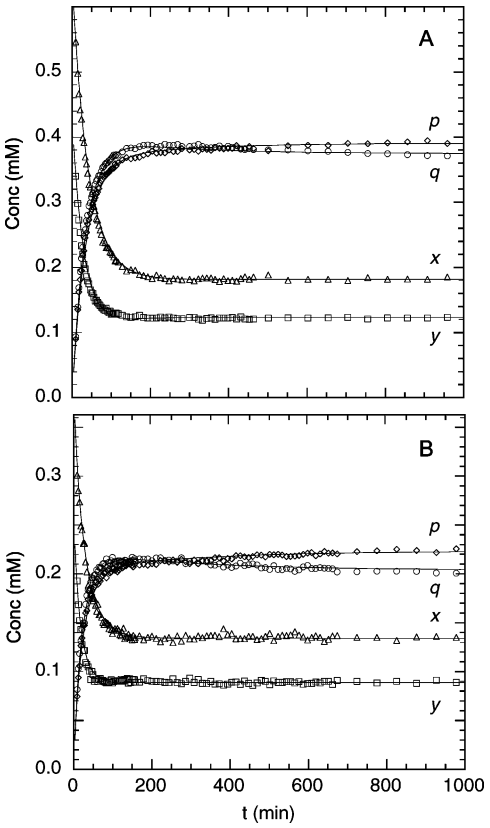


FIGURE 8: Time course of holoprotein concentrations in a typical NMR heme transfer experiment. In panel A, the initial concentrations of PE holocytochrome $b_5$ and wild-type apocytochrome $b_5$ were 1.07 and 0.91 mM, respectively. The instantaneous concentrations were obtained by simulation of spectra collected at regular intervals as described in the Materials and Methods. Curves labeled x and y pertain to the concentrations of the A and B heme isomers of the donor (PE) protein, respectively; curves p and q pertain to the concentrations of the A and B isomers of the acceptor (WT) protein, respectively. Panel B presents the same experiment with 0.65 mM PE holocytochrome $b_5$ and 0.48 mM wild-type apocytochrome $b_5$. The solid lines represent simulations of the data according to the mechanism provided in the Materials and Methods. Only the rate of loss of heme from the donor protein could be obtained reliably from the data.

to form A. Also noteworthy is the rate at which equilibration takes place in the wild-type holoprotein under these conditions. Although this rate is slow, it is faster than that in solutions containing only reconstituted wild-type holoprotein.

As pointed out above, the distribution of the heme group between wild-type and PE proteins at equilibrium and knowledge of the protein concentrations should allow for a measurement of relative heme affinities (eq 6). PE cytochrome $b_5$ had a heme affinity lower than that of wild-type cytochrome $b_5$ by a factor of at least 10. Experimental error in the measurement of concentrations prevented a definitive determination of the ratio.

*PE Holocytochrome $b_5$ Plus P81A Apocytochrome $b_5$.* The heme transfer from PE holocytochrome $b_5$ to P81A apocytochrome $b_5$ was also consistent with a rate-limiting step corresponding to the release of the heme from the donor protein. P81A apocytochrome $b_5$ was the least stable of all apoprotein variants studied here, but the heme affinity obtained from the equilibrated mixtures was found to be in favor of P81A cytochrome $b_5$ polypeptide although lower than that of the wild-type protein.

*Wild-type Holocytochrome $b_5$ Plus P81A Apocytochrome $b_5$.* This combination was not experimentally favorable because of the similarity of the holoprotein spectra and the high heme affinity (slow $k_{off}$) of these two proteins. Only minor amounts of P81A holocytochrome $b_5$ were detected after incubation of the mixture over 24 h.

*P81A Holocytochrome $b_5$ Plus PE Apocytochrome $b_5$.* The heme transfer from P81A holocytochrome $b_5$ to PE apocytochrome $b_5$ served as a control experiment. A slow reaction was expected because of the comparatively high affinity of P81A holocytochrome $b_5$ (slow $k_{off}$). After more than 24 h at 25 °C, there was evidence for the formation of some PE holocytochrome $b_5$; however, the concentration of the latter was too low for quantification.

With the heme transfer experiments, the following affinity order was established: wild-type > P81A > PE. The D60R variant was expected to rank with the wild-type protein based on the similarity of apo and holo stabilities and was not tested. The shortcoming of these experiments is in the need for accurate protein concentration measurements. On the other hand, NMR spectroscopy brought to light an unsuspected feature of the transfer, by which the thermodynamically disfavored heme isomer can be formed in excess of the favored one. The mechanism for this imbalance is unclear because the structural data collected on the apoprotein do not suggest that this species should be able to discriminate between the two heme orientations. The range of concentration that could be explored with this method was too narrow to provide unequivocal indication of direct protein−protein transfer.

*Effect of Sequence Alterations.* In the rat microsomal holoprotein, Asp60 is exposed to solvent and does not appear to form strong interactions with other side chains. However, it is near acidic residues Glu56 and Glu59. Inspection of cytochrome $b_5$ primary structures having two histidines as axial ligands (members of Pfam accession number PF00173) shows that position 60 accepts side chains such as valine, arginine, and glycine. The D60R holoprotein studied here had a $T_m$ higher than that of the wild-type holoprotein. This may be the result of reduced electrostatic repulsions in the *H* state. In this view, state a could be both structurally and thermodynamically unchanged by the mutation, while the maximum affinity, represented by the dashed arrow in Figure 1B, would be enhanced. This interpretation was set forth for the increased stability of the E48A/D60A cytochrome $b_5$ mutant (*35*). An alternative interpretation calls for an apoprotein with folded α4, making state *a* structurally closer to state *H* and decreasing the entropic cost of induced refolding upon heme binding. Two comments are in order. First, an increase in α4 helicity is not necessarily expected to change the stability of state *a*; in the wild-type protein, α4 is outside of the cooperative unit the structural dissipation of which is assessed in the apoprotein denaturation experiments, and the replacement may not extend this unit. Second, an increase in helicity in α4 would result in a change in MRE that would be difficult to measure accurately (*55*); the apoprotein CD spectrum was inconclusive in this regard.

The double sequence perturbation introduced in PE cytochrome $b_5$ was intended to disfavor the formation of α4 and resulted in a holoprotein with altered NMR spectral properties. Interestingly, the far-UV CD spectrum of the holoprotein was not affected by the change in sequence.

Heme binding was sufficiently strong to prevent loss during purification, and excess cyanide ions did not displace the axial histidine(s). The cytochrome $b_5$ sequence data indicate that major changes are tolerated in α4. Thus, position 57 can be occupied by a proline (for which there are more occurrences than the wild-type asparagine), and in several cases, the number of residues separating the well-conserved Phe58 and the axial His63 vary. The decrease in net heme affinity evident from transfer of the prosthetic group from PE cytochrome $b_5$ to the wild-type apoprotein raises a question about some of the naturally occurring proteins with modified α4, whether they also have a large heme dissociation constant or their sequence is otherwise altered to compensate for this potentially unfavorable trait.

The apparent stabilities of PE and wild-type apocytochromes were similar, but those of the holoproteins were not with a PE holoprotein destabilization reflecting either improved nonspecific heme binding or deteriorated specific binding (or both). The ratio of heme dissociation constants (eq 6, PE/wild-type) of 10 (corresponding to a $\Delta\Delta G°$ of ~6 kJ mol$^{-1}$) favored an effect on specific binding. A structural explanation in this case would call for similar extent of residual structure in the wild-type and PE *ah* state, and a binding site incapable of assuming the same strong interactions with the heme group as in the wild-type protein. The thermal denaturation of secondary structure prior to heme loss supported this interpretation.

Position 81 is not included in the definition of cytochrome $b_5$ Pfam. A limited comparison of primary structures demonstrates variability at site 81, including instances of serine, threonine, and glutamic acid. In contrast to D60R and PE cytochrome $b_5$, which presented apoprotein features similar to the wild-type polypeptide, the type II mutant P81A had decreased apo- and holoprotein stability. In this case, the low apoprotein stability is expected to be reflected in the denaturation behavior of the holoprotein. After adjustment for this influence, the data suggested a reduction of the difference between specific and nonspecific binding compared to the wild-type protein. This is difficult to rationalize since P81A cytochrome $b_5$ illustrates a replacement that does not contact the heme (Figure 2). The properties of the apoprotein might therefore play a role not only in the apparent stability of the holoprotein but also in controlling heme affinity. This role would be modest in the P81A cytochrome: if the ~6 kJ mol$^{-1}$ destabilization observed in the apoprotein state were converted into an equivalent decrease in heme affinity, one would expect PE and P81A cytochromes to have the same affinity, which was not the case. Studies of the wild-type apoprotein have shown that the dynamics of α6, an imperfect helix N-capped by His80, are altered by the presence of the heme (*25*). A cascade of contacts between site 81 and the heme, for example, those involving the intervening Tyr6 and Glu78, would be responsible for the long-range communication resulting in weaker heme binding.

A limited study of protein stability and heme affinity in sperm whale myoglobin has revealed a strong correlation between heme binding and holoprotein denaturation behavior but not apoprotein denaturation properties (*37*). This conclusion was based on a pair of substitutions targeting residues in direct contact with the heme group, V68T and H97D. The first mutant has features of type I (contact with heme) and type II (folded in the apoprotein) cytochrome $b_5$ variants, whereas the second is type I (contact with the heme and unfolded in the apoprotein) (*10*). The cytochrome system is simpler in two ways: it has bis-histidine coordination of the iron ion, and the denaturation of the apoprotein follows an apparent two-state behavior. The perturbations that were investigated here were proximal to and remote from the heme group. A behavior similar to that of myoglobin was observed: the ill-defined *uh* and *ah* states increased the complexity of the energetic relationships normally considered for small organic ligands, but they introduced an additional mechanism for decoupling of stability and affinity. Moreover, the type II mutation exposed a relation between apoprotein stability and heme affinity, suggesting the presence of "hot spots" in the structure and action at a distance akin to an allosteric effect. Additional work is in progress to map those sites for which long-range effects are detectable as in P81A cytochrome $b_5$ and define further the role of apoprotein stability in modulating heme affinity.

## ACKNOWLEDGMENT

The authors thank Dr. Osman Bilsel for providing the program SAVUKA, Dr. Dan Jones for the mass spectrometry analyses, Elizabeth Baldauf and Dr. Michael Mayer for initiating the project, and Jane Knappenberger and Dr. Christopher Falzone for useful discussions. Figure 2 was prepared with MOLSCRIPT (*56*).

## REFERENCES

1. Chothia, C., Lesk, A. M., Dodson, G. G., and Hodgkin, D. C. (1983) Transmission of conformational change in insulin, *Nature 302*, 500−505.
2. Gerstein, M., Lesk, A. M., and Chothia, C. (1994) Structural mechanisms for domain movements in proteins, *Biochemistry 33*, 6739−6749.
3. Yu, E. W., and Koshland, D. E., Jr. (2001) Propagating conformational changes over long (and short) distances in proteins, *Proc. Natl. Acad. Sci. U.S.A. 98*, 9517−9520.
4. Luque, I., and Freire, E. (2000) Structural stability of binding sites: consequences for binding affinity and allosteric effects, *Proteins Suppl. 4*, 63−71.
5. Leulliot, N., and Varani, G. (2001) Current topics in RNA-protein recognition: control of specificity and biological function through induced fit and conformational capture, *Biochemistry 40*, 7947−7956.
6. Breslow, E., Beychok, S., Hardman, K. D., and Gurd, F. R. N. (1965) Relative conformations of sperm whale metmyoglobin and apomyoglobin in solution, *J. Biol. Chem. 240*, 304−309.
7. Moore, C. D., and Lecomte, J. T. (1990) Structural properties of apocytochrome $b_5$: presence of a stable native core, *Biochemistry 29*, 1984−1989.
8. Robinson, C. R., Liu, Y., O'Brien, R., Sligar, S. G., and Sturtevant, J. M. (1998) A differential scanning calorimetric study of the thermal unfolding of apo- and holo-cytochrome $b_{562}$, *Protein Sci. 7*, 961−965.
9. Sugishima, M., Sakamoto, H., Kakuta, Y., Omata, Y., Hayashi, S., Noguchi, M., and Fukuyama, K. (2002) Crystal structure of rat apo-heme oxygenase-1 (HO-1): mechanism of heme binding in HO-1 inferred from structural comparison of the apo and heme complex forms, *Biochemistry 41*, 7293−7300.
10. Lecomte, J. T. J., Sukits, S. F., Bhattacharya, S., and Falzone, C. J. (1999) Conformational properties of native sperm whale apomyoglobin in solution, *Protein Sci. 8*, 1484−1491.
11. Lecomte, J. T. J., Scott, N. L., Vu, B. C., and Falzone, C. J. (2001) Binding of ferric heme by the recombinant globin from the cyanobacterium *Synechocystis* sp. PCC 6803, *Biochemistry 40*, 6541−6552.
12. Izadi, N., Henry, Y., Haladjian, J., Goldberg, M. E., Wandersman, C., Delepierre, M., and Lecroisey, A. (1997) Purification and

characterization of an extracellular heme-binding protein, HasA, involved in heme iron acquisition, *Biochemistry 36*, 7050−7057.
13. Hargrove, M. S., Barrick, D., and Olson, J. S. (1996) The association rate constant for heme binding to globin is independent of protein structure, *Biochemistry 35*, 11293−11299.
14. Mathews, F. S., Czerwinski, E. W., and Argos, P. (1979) The X-ray crystallographic structure of calf liver cytochrome $b_5$, *The Porphyrins*, Vol. 7, Academic Press, New York.
15. Arnesano, F., Banci, L., Bertini, I., and Felli, I. C. (1998) The solution structure of oxidized rat microsomal cytochrome $b_5$, *Biochemistry 37*, 173−184.
16. Falzone, C. J., Wang, Y., Vu, B. C., Scott, N. L., Bhattacharya, S., and Lecomte, J. T. (2001) Structural and dynamic perturbations induced by heme binding in cytochrome $b_5$, *Biochemistry 40*, 4879−4891.
17. Bhattacharya, S., Falzone, C. J., and Lecomte, J. T. (1999) Backbone dynamics of apocytochrome $b_5$ in its native, partially folded state, *Biochemistry 38*, 2577−2589.
18. Falzone, C. J., Mayer, M. R., Whiteman, E. L., Moore, C. D., and Lecomte, J. T. (1996) Design challenges for hemoproteins: the solution structure of apocytochrome $b_5$, *Biochemistry 35*, 6519−6526.
19. Moore, C. D., Al-Misky, O. N., and Lecomte, J. T. J. (1991) Similarities in structure between holocytochrome $b_5$ and apocytochrome $b_5$: NMR studies of the histidine residues, *Biochemistry 30*, 8357−8365.
20. Ihara, M., Takahashi, S., Ishimori, K., and Morishima, I. (2000) Functions of fluctuation in the heme-binding loops of cytochrome $b_5$ revealed in the process of heme incorporation, *Biochemistry 39*, 5961−5970.
21. Pfeil, W. (1993) Thermodynamics of apocytochrome $b_5$ unfolding, *Protein Sci. 2*, 1497−1501.
22. Constans, A. J., Mayer, M. R., Sukits, S. F., and Lecomte, J. T. (1998) A test of the relationship between sequence and structure in proteins: excision of the heme binding site in apocytochrome $b_5$, *Protein Sci. 7*, 1983−1993.
23. Cowley, A. B., Altuve, A., Kuchment, O., Terzyan, S., Zhang, X., Rivera, M., and Benson, D. R. (2002) Toward engineering the stability and hemin-binding properties of microsomal cytochromes $b_5$ into rat outer mitochondrial membrane cytochrome $b_5$: examining the influence of residues 25 and 71, *Biochemistry 41*, 11566−11581.
24. Wang, W. H., Lu, J. X., Yao, P., Xie, Y., and Huang, Z. X. (2003) The distinct heme coordination environments and heme-binding stabilities of His39Ser and His39Cys mutants of cytochrome $b_5$, *Protein Eng. 16*, 1047−1054.
25. Lecomte, J. T. J., and Moore, C. D. (1991) Helix formation in apocytochrome $b_5$: the role of a neutral histidine at the N-cap position, *J. Am. Chem. Soc. 113*, 9663−9665.
26. Beck von Bodman, S., Schuler, M. A., Jollie, D. R., and Sligar, S. G. (1986) Synthesis, bacterial expression, and mutagenesis of the gene coding for mammalian cytochrome $b_5$, *Proc. Natl. Acad. Sci. U.S.A. 83*, 9443−9447.
27. de Duve, C. (1948) A spectrophotometric method for the simultaneous determination of myoglobin and hemoglobin in extracts of human muscle, *Acta Chem. Scan. 2*, 264−289.
28. Antonini, E., and Brunori, M. (1971) *Hemoglobin and myoglobin in their reactions with ligands*, Vol. 12, North-Holland, Amsterdam.
29. Teale, F. W. (1959) Cleavage of the haem-protein link by acid methylethylketone, *Biochim. Biophys. Acta 35*, 543.
30. Strittmatter, P. (1960) The nature of the heme binding in microsomal cytochrome $b_5$, *J. Biol. Chem. 235*, 2492−2497.
31. Becktel, W. J., and Schellman, J. A. (1987) Protein stability curves, *Biopolymers 26*, 1859−1877.
32. Pace, C. N., and Laurents, D. V. (1989) A new method for determining the heat capacity change for protein folding, *Biochemistry 28*, 2520−2525.
33. Pace, C. N., Shirley, B. A., and Thomson, J. A. (1989) *Protein structure: a practical approach*, IRL Press, Oxford, U.K., New York.
34. Pace, C. N. (1986) Determination and analysis of urea and guanidine hydrochloride denaturation curves, *Methods Enzymol. 131*, 266−280.
35. Wang, Y. H., Ren, Y., Wang, W. H., Xie, Y., and Huang, Z. X. (2001) The regulation of surface charged residues on the properties of cytochrome $b_5$, *J. Protein Chem. 20*, 487−493.
36. Bilsel, O., Zitzewitz, J. A., Bowers, K. E., and Matthews, C. R. (1999) Folding mechanism of the α-subunit of tryptophan synthase, an $\alpha/\beta$ barrel protein: global analysis highlights the interconversion of multiple native, intermediate, and unfolded forms through parallel channels, *Biochemistry 38*, 1018−1029.
37. Hargrove, M. S., and Olson, J. S. (1996) The stability of holomyoglobin is determined by heme affinity, *Biochemistry 35*, 11310−11318.
38. Piotto, M., Saudek, V., and Sklenár, V. (1992) Gradient-tailored excitation for single-quantum NMR spectroscopy of aqueous solutions, *J. Biomol. NMR 2*, 661−665.
39. Sklenár, V., Piotto, M., Leppik, R., and Saudek, V. (1993) Gradient-tailored water suppression for $^1$H-$^{15}$N HSQC experiments optimized to retain full sensitivity, *J. Magn. Reson. 102*, 241−245.
40. Massiot, D., Fayon, F., Capron, M., King, I., Le Calve, S., Alonso, B., Durand, J. O., Bujoli, B., Gan, Z. H., and Hoatson, G. (2002) Modelling one- and two-dimensional solid-state NMR spectra, *Magn. Reson. Chem. 40*, 70−76.
41. Barshop, B. A., Wrenn, R. F., and Frieden, C. (1983) Analysis of numerical methods for computer simulation of kinetic processes: development of KINSIM-a flexible, portable system, *Anal. Biochem. 130*, 134−145.
42. Dang, Q., and Frieden, C. (1997) New PC versions of the kinetic-simulation and fitting programs, KINSIM and FITSIM, *Trends Biochem. Sci. 22*, 317.
43. Lee, K. B., La Mar, G. N., Kehres, L. A., Fujinari, E. M., Smith, K. M., Pochapsky, T. C., and Sligar, S. G. (1990) $^1$H NMR study of the influence of hydrophobic contacts on protein-prosthetic group recognition in bovine and rat ferricytochrome $b_5$, *Biochemistry 29*, 9623−9631.
44. Guiles, R. D., Basus, V. J., Sarma, S., Malpure, S., Fox, K. M., Kuntz, I. D., and Waskell, L. (1993) Novel heteronuclear methods of assignment transfer from a diamagnetic to a paramagnetic protein: application to rat cytochrome $b_5$, *Biochemistry 32*, 8329−8340.
45. La Mar, G. N., Burns, P. D., Jackson, J. T., Smith, K. M., Langry, K. C., and Strittmatter, P. (1981) Proton magnetic resonance determination of the relative heme orientations in disordered native and reconstituted ferricytochrome $b_5$. Assignment of heme resonances by deuterium labeling, *J. Biol. Chem. 256*, 6075−6079.
46. Lee, K. B., La Mar, G. N., Mansfield, K. E., Smith, K. M., Pochapsky, T. C., and Sligar, S. G. (1993) Interpretation of hyperfine shift patterns in ferricytochromes $b_5$ in terms of angular position of the heme: a sensitive probe for peripheral heme protein interactions, *Biochim. Biophys. Acta 1202*, 189−199.
47. Sarma, S., DiGate, R. J., Banville, D. L., and Guiles, R. D. (1996) $^1$H, $^{13}$C and $^{15}$N NMR assignments and secondary structure of the paramagnetic form of rat cytochrome $b_5$, *J. Biomol. NMR 8*, 171−183.
48. Robinson, C. R., Liu, Y., Thomson, J. A., Sturtevant, J. M., and Sligar, S. G. (1997) Energetics of heme binding to native and denatured states of cytochrome $b_{562}$, *Biochemistry 36*, 16141−16146.
49. Shen, L. L., and Hermans, J., Jr. (1972) Kinetics of conformation change of sperm-whale myoglobin. III. Folding and unfolding of apomyoglobin and the suggested overall mechanism, *Biochemistry 11*, 1845−1849.
50. Shen, L. L., and Hermans, J., Jr. (1972) Kinetics of conformation change of sperm-whale myoglobin. II. Characterization of the rapidly and slowly formed denatured species (D and D*), *Biochemistry 11*, 1842−1844.
51. Shen, L. L., and Hermans, J., Jr. (1972) Kinetics of conformation change of sperm-whale myoglobin. I. Folding and unfolding of metmyoglobin following pH jump, *Biochemistry 11*, 1836−1841.
52. Muñoz, V., and Serrano, L. (1995) Elucidating the folding problem of helical peptides using empirical parameters. II. Helix macrodipole effects and rational modification of the helical content of natural peptides, *J. Mol. Biol. 245*, 275−296.
53. Muñoz, V., and Serrano, L. (1995) Elucidating the folding problem of helical peptides using empirical parameters. III. Temperature and pH dependence, *J. Mol. Biol. 245*, 297−308.
54. La Mar, G. N., Satterlee, J. D., and de Ropp, J. S. (1999) in *The Porphyrin Handbook* (Smith, K. M., Kadish, K., and Guilard, R., Eds.) pp 185−298, Academic Press, Burlington, MA.
55. Johnson, W. C., Jr. (1990) Protein secondary structure and circular dichroism: a practical guide, *Proteins 7*, 205−214.
56. Kraulis, P. (1991) MOLSCRIPT: A program to produce both detailed and schematic plots of protein structures, *J. Appl. Crystallogr. 24*, 946−950.

BI0488956